Engineered Science
DOI: https://dx.doi.org/10.30919/es1168

Synthesis, Pharmacokinetic, Molecular Docking, and Molecular Dynamics Simulation of 2-Styrylchromone Derivatives as Potential Inhibitor of Human Kinesin Eg5

Alfinda Novi Kristanti[1, 2,*] Nanik Siti Aminaha,[2] Imam Siswanto,[1, 3] Andika Pramudya Wardana,[4] Muhammad Ikhlas Abdjan,[1] Ana Rizki Khoirunisak[1] and Evi Noviana[1]

Abstract

Synthesis and characterization of 2-styrylchromone derivatives had been done through aldol condensation between 2-methylchromone and various cinnamaldehyde with modified substituent groups on the benzene ring, such as –Br and –OCH_3. Pharmacokinetic studies provide some information on the drug-likeness, bioavailability, and ADMET (absorption, distribution, metabolism, excretion, and toxicity) properties of these 2-styrylchromone derivatives. Meanwhile, a structure-based approach was performed to study the potential of 2-styrylchromones as an inhibitor of the kinesin Eg5. The activity of kinesin Eg5 was found in the regulation of the mitosis phase on cancer cells, so it has a promising target potential in cancer therapy. The results show that MT2 and MT3 have promising potential as Eg5 kinesin inhibitors from a thermodynamic aspect. The prediction of binding free energy (ΔG_{bind}) using the Molecular Mechanics-Generalized Born Surface Area (MM-GBSA) approach shows the ΔG_{bind} (kcal mol^{-1}) of MT3-Eg5: -33.89 ± 0.28 and MT4-Eg5: -21.88 ± 0.22. Besides, Energy decomposition ($\Delta G_{bind}^{residue}$) presented 12 key binding residues which were identified as responsible for the interaction with inhibitors, such as E100, R103, S104, P105, W111, I120, P121, Y195, L198, E199, A202, and A203. The obtained results demonstrated how 2-styrylchromone derivatives could be considered against the kinesin Eg5 at the molecular level.

Keywords: 2-styrylchromone; Human Kinesin Eg5; Computational study; ADMET.
Received: 29 January 2024; Revised: 09 May 2024; Accepted: 21 May 2024.
Article type: Research article.

1. Introduction

Cancer is a disease caused by the growth of abnormal cells that cause damage to other normal tissues in the human body.[1] The diagnostic case study showed that female breast cancer (11.7%) was the most common (2.3 million new cases) compared to other cancer cases, such as lung (11.4%), colorectal (10.0%), prostate (7.3%), and stomach (5.6%) cancers.[2] Currently, cancer death cases still occur in various parts of the world. Therefore, the development of drugs and cancer cell therapy is a major concern in the reduction of cancer death cases.[3,4]

Cancer cell therapy by targeting certain proteins that play a crucial role in the mechanism of cell development has been widely applied.[5,6] One of them is targeting the kinesin Eg5 protein, which plays an active role in the life cycle of cancer cells.[7–9] Kinesin Eg5 (also known as KSP) is a spindle motor protein that plays a specific role in the mitosis phase (M) in the development of cancer cells.[8,9] This protein moves along microtubules (MTs) using hydrolyzed adenosine triphosphate (ATP) energy, which functions as a cargo transport cell.[7] Additionally, several kinesin proteins have been found to play roles during the mitotic phase.[10] The kinesin Eg5 inhibition can disrupt the mitotic process in cancer cells, which probably can stop their life cycle. Therefore, kinesin protein is a potential target in cancer therapy.[11,12] Besides, kinesin Eg5 inhibition is promising because it improves the side effects profile during cancer therapy.[13,14]

The efficacious kinesin Eg5 inhibitor is ispinesib, which

[1] *Department of Chemistry, Faculty of Science and Technology, Universitas Airlangga, Komplek Kampus C UNAIR, Jl. Mulyorejo, Surabaya 60115, Indonesia.*
[2] *Biotechnology of Tropical Medicinal Plants Research Group, Universitas Airlangga, Jawa Timur 60132, Indonesia.*
[3] *Bioinformatic Laboratory, UCoE Research Center for Bio-Molecule Engineering, Universitas Airlangga, Surabaya 60115, Indonesia.*
[4] *Department of Chemistry, Faculty of Mathematics and Natural Sciences, State University of Surabaya, Lakarsantri 60213, Indonesia.*
**Email:* alfinda-n-k@fst.unair.ac.id (A. N. Kristanti)

shows good anticancer activity.[14] Therefore, the development of a kinesin Eg5 inhibitor was carried out based on the ispinesib structure as a reference (Fig. S1). One of them is chromone compounds, which have a similar structure to ispinesib in two rings A and C (Fig. 1). The structure similarity is expected to have a similar inhibitory mechanism for kinesin Eg5 protein. Therefore, the synthesis of chromone derivatives is the main focus of this research. Previous reports stated that chromone derivatives have potential as Eg5 kinesin inhibitors.[15] Previous researchers have proven that chromone derivatives have various pharmacological properties.[16] Some chromone derivatives have been investigated for their anticancer activity, including the thiochroman-4-one, which shows higher anticancer activity than melphalan as the standard drug (a chemotherapy drug used to treat ovarian cancer and amyloidosis).[17] In other studies, benzylchroman-4-one and its derivatives have been identified as anticancer, antioxidant, and antituberculosis.[18] Chromen-4-yl phosphate derivative has activity against cancer cells.[19] Additionally, chromen-2-on derivatives can be used for breast cancer chemotherapy.[20]

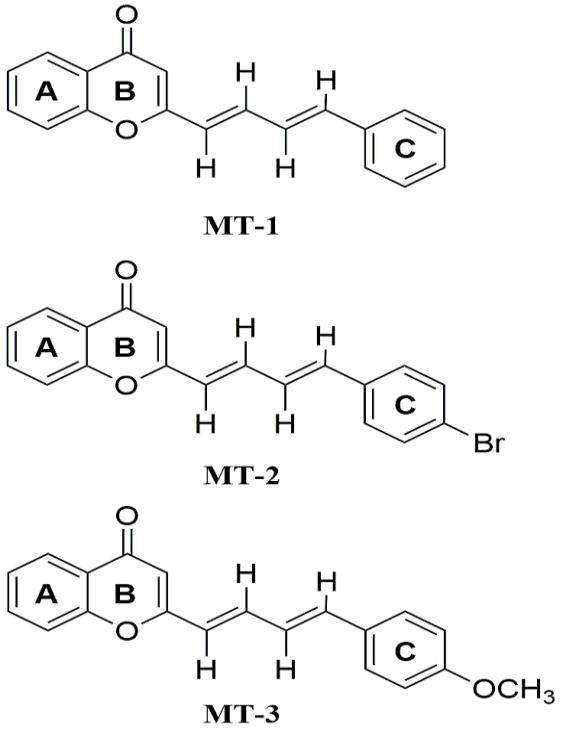

Fig. 1 Chemical structure of synthesized 2-styrylchromone derivatives.

Molecular studies aim to investigate the interaction of small molecules with kinesin Eg5 protein at the molecular level. This study provides information to understand the inhibition mechanism of chromone derivatives at the kinesin Eg5 binding site.[21] The alternative method used is the based-structure approach through a combination of molecular docking and molecular dynamics (MD) simulation.[22,23] Moreover, this approach has been shown to have advantages in the development of inhibitors.[12,24] The theoretical analysis is useful for designing the candidate inhibitors. Some of the variables presented in this work are the synthesis of 2-styrylchromone derivatives using the aldol condensation reaction and their characterization. Meanwhile, pharmacokinetic studies of synthetic compounds are performed to determine their criteria as good drug candidates. Moreover, the combination of molecular docking and molecular dynamics (MD) simulation provides molecular insight into the potential of synthesized 2-styrylchromone derivatives against the Eg5 protein, which is responsible for cancer cell growth as described above. Previous research showed that the synthesis of 2-styrylchromone was carried out with various benzaldehyde reagents.[21] In this work, we synthesized 2-styrylchromone derivatives using *trans*-cinnamaldehyde, *p*-bromo cinnamaldehyde, and *p*-methoxy cinnamaldehyde reagents. Moreover, the combination of molecular docking studies and MD simulations regarding the activity of synthesized 2-styrylchromones against kinesin Eg5 at the molecular level is the first to be reported in this work. Therefore, several variables measured in this work would provide novelty and information regarding the design of chromone structure-based Eg5 kinesin inhibitor.

2. Experimental section

2.1 Materials

The materials used are *trans*-cinnamaldehyde (Merck), 4-bromocinnamaldehyde (Merck), 4-methoxycinnamaldehyde (Merck), 2-hydroxyacetophenone (Sigma-Aldrich), sodium, HCl 0.5N, ethyl acetate, *p*-toluenesulfonic acid (*p*TSA) (Merck), ethanol (Merck), *n*-hexane (Merck), ethyl acetate (Merck), chloroform (Merck), methanol (Merck), aquadest, and NaOH 40%.

2.2 Synthesis and characterization

The synthesis of MT-1 was obtained through an aldol condensation reaction between 2-methylchromone and *trans*-cinnamaldehyde. The 2-methylchromone was first synthesized according to the procedure as stated in reference.[21] A total of 0.5 mmol of 2-methylchromone was reacted with 0.55 mmol of *trans*-cynamaldehyde, followed by the addition of 8 mL of ethanol and 0.5 mL of 1 M NaOH as a catalyst. Then, the mixture was stirred at < 5°C for ± 1 hour. After 1 hour, the reaction was continued at room temperature for 3 hours. The reaction products were recrystallized to obtain MT-1 compound. The orange solid formed was filtered using a Buchner funnel and recrystallized with a single solvent of ethanol. Next, its purity was tested using thin layer chromatography (TLC) with three eluent systems. The yield obtained from the synthesis of MT-1 was 35.4 mg (25.6%). The melting point data for the MT-1 compound is 144–146 °C. This procedure was repeated by replacing the *trans*-cinnamaldehyde with *p*-bromo cinnamaldehyde and *p*-methoxy cinnamaldehyde to obtain MT-2 and MT-3, respectively. The MT-2 was recrystallized by using methanol with a yield of 33.92%. The melting point data for the MT-2

compound is 180-182 ºC. Meanwhile, the MT-3 compound formed was not pure. So, it was necessary to separate it using column chromatography to purify the compound. Elution in column chromatography was carried out using the eluent n-hexane: ethyl acetate in a ratio of 25:1. After the compound was purified by column chromatography, its purity was tested using TLC with three different eluents. The yield obtained from the MT-2 synthesis was 45.34%. The melting point data for compound MT-3 is 137-139 ºC. These synthesized compounds were characterized by melting point (Buchi M-560 melting point apparatus), UV-Vis spectrophotometer (Shimadzu UV-1800), FTIR (Shimadzu IR Tracer-100), NMR (JEOL JNM-ECS 400), and MS (JEOL 600H-1).

2.3 Drug-likeness, bioavailability, and ADMET prediction

Pharmacokinetics prediction for inhibitors as drug candidates were predicted by the web service SwissADME[25] and pkCSM.[26] The drug-likeness, bioavailability, and ADMET calculations were performed using a 2D structure (SMILES format). Drug-likeness and bioavailability criteria were calculated based on several rules, including Lipinski,[27] Ghose,[28] Veber,[29] Egan,[30] and Muegge[31] rules. Meanwhile, the prediction of ADMET aims to study the biological activity of drug candidates in the body.

2.4 Inhibitor and receptor preparation

The target protein uses the crystal structure of the human kinesin Eg5 obtained from the protein data bank (PDB ID: 4AP0). The crystal complex contained ispinesib inhibitor (PDB ID: G7X) as a native ligand located on the active site of the kinesin Eg5. Homology modeling was carried out to refine the missing residue in the target protein using the Modeller package. The G7X and amino acid residues (receptors) were extracted from the crystal structure kinesin Eg5 using the Chimera version 1.13 package to obtain their initial coordinates. The G7X inhibitor was used as a control because it had an inhibitory activity of the kinesin Eg5 14. In addition, doxorubicin (PDB ID: DM2) was also used as a control (Fig. S1) in this study because of its known general anticancer activity.[32] Meanwhile, candidate inhibitors of 2-styrylchromones were calculated for electrostatic potential (ESP) charges using the DFT/B3LYP/6-31G(d,p) method. Finally, the AMBER force field (FF14SB) and Austin model 1-bond charge correction (AM1-BCC) were applied to ligands and receptors for parameter purposes, such as bonded, nonbonded, and charge.

2.5 Molecular docking and molecular dynamics simulation

All procedural molecular docking was performed by using the DOCK6 package. The grid-box is made based on the coordinates of selected spheres (radius: 10 Å) on the receptor active site. The rigid conformation with a grid score function approach is applied to perform the redocking process. The inhibitor-receptor scoring process (Eq. 1) takes place in a gas term with energy considerations in the form of van der Waals (E_{vdW}) and electrostatic (E_{ele}). The criteria for the success of the redocking process in determining the native ligand superposition is RMSD ≤ 2.0 Å.[33] Then, the docking inhibitor process uses the parameters used previously in the redocking process that meet the criteria.

$$\text{Grid-Score} = E_{vdW} + E_{ele} \quad (1)$$

The obtained coordinates of each complex from the docking process are integrated into the MD simulation using the General AMBER Force Field (GAFF).[34] The topology preparation of each system in the form of ligand, receptor, complex, receptor-solvated, and complex-solvated using the tleap tool available in the AMBER18 package. The solvent model used is TIP3P water solvent and sodium counterions to neutralize the system (Na^+ randomly added). The minimization process is carried out on water molecules and counterions (steepest descent: 1500 steps and conjugate gradient: 500 steps). Next, the complex was minimized by 1500 steps of steepest descent and 500 steps of a conjugate gradient. Finally, the entire system was fully minimized by the same protocol. In this stage, the heating process is carried out gradually (10 K to 310 K) for 200 ps with a harmonic restraint of 30 kcal mol^{-1} $Å^{-2}$. The process was continued by system equilibrium stages with harmonic restraint of 30, 20, 10, and 5 kcal mol^{-1} $Å^{-2}$ for 1300 ps. Finally, the entire system is produced under the NPT ensemble (310 K and 1 atm) until reaching 100 ns. The whole simulation process is carried out to obtain trajectories from each system for further analysis.

2.6 Trajectories analysis

The conformational dynamics of each system were evaluated through system stability, compactness, and flexibility for 100 ns trajectories. Meanwhile, further analysis needs such as water accessibility, atom contact, hydrogen bonding, and binding free energy use the last 20 ns (80-100 ns) trajectories. Trajectories analysis used *cpptraj*[35] and *MMPBSA.py*[36] tools available in the AMBER18 package

Binding free energy (ΔG_{bind}) and energy decomposition ($\Delta G_{bind}^{residue}$) were calculated using the Molecular Mechanics-Generalized Born Surface Area (MM-GBSA) approach. Some of the key parameters used are the Generalized Born solvation model: 2, the concentration of mobile counterions in solution: 0.00 M, and nonpolar contribution of solvation free energy: 0.0072. The determination of ΔG_{bind} is calculated by considering several parameters, including the gas term (ΔG_{gas}), solvation term (ΔG_{sol}), and entropy change ($-T\Delta S$), which are described in Eq. 2. However, $-T\Delta S$ is ignored because of the large calculation costs and low prediction accuracy 37. In detail, the energy component of ΔG_{gas} is described in full in Eq. 3. In particular, energy bonded (ΔE_{bonded}) consists of bond, angle, and torsion energies, which have conformational energies of equal zero. Meanwhile, the energy component in ΔG_{sol} is the total of Generalized Born models (ΔG_{sol}^{ele}) and solvent-accessible surface area energy ($\Delta G_{sol}^{nonpolar}$) (Eq. 4). Finally, the free energy binding can be calculated in detail

using Eq. 5.

$$\Delta G_{bind} = \Delta G_{Gas} + \Delta G_{solv} - T\Delta S \quad (2)$$

$$\Delta G_{Gas} = \Delta E_{bonded} + \Delta E_{vdW} + \Delta E_{ele} \quad (3)$$

$$\Delta G_{Solv} = \Delta G_{sol}^{ele} + \Delta G_{sol}^{nonpolar} \quad (4)$$

$$\Delta G_{bind} = \Delta E_{vdW} + \Delta G_{sol}^{nonpolar} + \Delta E_{ele} + \Delta G_{sol}^{ele} \quad (5)$$

3. Results and discussion

3.1 Synthesis and characterization of 2-styrylchromones

The MT-1, MT-2, and MT-3 are compounds that have the same skeleton structure, namely 2-styrylchromone (Fig. 1). The structure of synthesized compounds were elucidated by spectroscopy methods.

2-((1E,3E)-4-fenilbuta-1,3-dien-1-il)-4H-kromen-4-on (MT-1): Orange solid (35.4 mg; 25.6%); m. p. = 144–146°C. Rf = 0.5 (*n*-hexane:ethyl acetate = 3:1); 0.25 (chloroform:*n*-hexane = 3:1); 0.6 (chloroform:ethyl acetate= 4:1). UV-Vis (MeOH) λ_{max} (nm) (log ε): 248 (4.11); 269 (4.06); 362 (4.46). FTIR (DFT, KBr, ν) cm^{-1}: 3055 (C-H sp^2); 1637 (C=O); 1614 (C=C alkene); 1490, 1564 (C=C aromatic); 1278 (Caryl–O–Cvinyl). ^{1}H-NMR (400 MHz, $CDCl_3$) δ 8.19 (dd, *J* = 7.9; 1.5 Hz; 1H); 7.67 (ddd, *J* = 8.6; 7.2; 1.7 Hz, 1H); 7.49 (dd, *J* = 8.3; 2.5 Hz, 2H); 7.44 (dd, *J* = 7.3, 2.7 Hz, 1H); 7.42 – 7.29 (m, 5H); 7.02 – 6.90 (m, 2H), 6.37 (d, *J* = 15.2 Hz, 1H); 6.26 (s, 1H). ^{13}C-NMR (100 MHz, $CDCl_3$) δ 178.5; 161.9; 156.1; 139.2; 137.5; 136.3; 133.8; 129.0; 129.0; 127.2; 125.8; 125.0; 124.2; 123.7; 117.9; 110.4 (Figs. S2-S5)

2-[(1E,3E)-4-(4-bromophenyl)buta-1,3-dien-1-yl)-4H-chromen-4-one (MT-2): Yellow solid (38.8 mg; 33.92%); m. p. = 180-182 °C. Rf = 0.30 (*n*-hexane:dichloromethane= 1:4); 0.32 (*n*-hexane:ethyl acetate= 3:1); 0.65 (dichloromethane:ethyl acetate= 3:1). UV-Vis (MeOH) λ_{max} (nm): 247.5; 274.5; 361.5. FTIR (DFR, KBr, ν) cm^{-1}: 3059 (C-H sp^2); 1651 (C=O); 1612 (C=C alkene); 1485 (C=C aromatic); 1292 (Caryl-O-Cvinyl); 1070 (C-Br). ^{1}H-NMR (400 MHz, $CDCl_3$) δ 8.18 (dd, *J* = 7.9, 1.6 Hz, 1H), 7.68 (ddd, *J* = 8.6, 7.2, 1.6 Hz, 1H), 7.51 (dd, *J* =8.5, 1.9 Hz, 1H), 7.42 (d, *J* = 10.2 Hz, 2H), 7.40 – 7.36 (m, 2H), 7.35 (d, *J* = 8.5 Hz, 2H), 6.99 – 6.86 (m, 2H), 6.39 (d, *J* = 15.2 Hz, 1H), 6.27 (s, 1H). ^{13}C-NMR (100 MHz, $CDCl_3$) δ 161.3, 157.9, 137.4, 136.7, 133.5, 134.9, 131.8, 128.2, 127.4, 125.4, 124.8, 124.1, 124.0, 123.9, 117.5, 110.3 (Figs. S6-S9).

2-[(1E,3E)-4-(4-metoxyphenyl)buta-1,3-dien-1-yl)-4H-chromen-4-on (MT-3): Yellow solid (30.00 mg; 45.34%); m.p.= 137-139 °C. Rf = 0.30 (*n*-hexane:dichloromethane= 1:4); 0.66 (*n*-hexane:ethyl acetate= 3:1); 0.69 (chloroform:ethyl acetate= 3:1). UV-Vis (MeOH) λ_{max} (nm): 256.5; 282.5; 381. FTIR (DFR, KBr, ν) cm^{-1}: 3059 (C-H sp^2); 2994 (C-H sp^3); 1649 (C=O); 1625 (C=C alkene); 1597 (C=C aromatic); 1261 (Caryl-O-Cvinyl). ^{1}H-NMR (400 MHz, $CDCl_3$) δ 8.18 (dd, *J* = 7.9, 1.6 Hz, 1H), 7.67 (ddd, *J* = 8.6, 7.1, 1.7 Hz, 1H), 7.49 (dd, *J* = 8.5, 1.1 Hz, 1H), 7.44 (d, *J* = 9.0 Hz, 2H), 7.41 (s, 1H), 7.38 (ddd, *J* = 8.0, 7.0, 1.1 Hz, 1H), 6.94 – 6.88 (m, 1H), 6.85 (d, *J* = 10.1 Hz, 2H); 6.87-6.83 (m, 1), 6.32 (d, *J* = 15.3 Hz, 1H), 6.29 (s, 1H), 3.84 (s, 3H). ^{13}C-NMR (100 MHz, $CDCl_3$) δ 178, 162.2, 155.7, 140.5, 138.8, 136.1, 133.5, 128.5, 128.4, 125.4, 125.0, 124.7, 123.0, 121.9, 117.5, 114.1, 109.8, 55.1 (Figs. S10-S13).

3.2 Pharmacokinetic properties

Pharmacokinetic studies aim to provide a more detailed description of the ability of a compound that has potential as a drug candidate. This potential must meet several criteria, such as drug-likeness, bioavailability, and ADMET. Therefore, the initial study of these variables is an important point in understanding the pharmacokinetic properties of a compound based on its structure.

Prediction of drug-likeness and bioavailability of 2-styrylchromones showed good permeability compared to G7X and DM2 by fulfilling several rules, such as Lipinski, Ghose, Veber, Egan, and Muegge (Table S1). As reported, G7X and DM2 are known drugs for cancer treatment. The MT-1 and MT-3 compounds showed no violations. Meanwhile, the MT-2 compound shows one violation of Egan's rule, namely the XlogP3 value of 5.8. Overall, 2-styrylchromones showed good drug-likeness criteria with total violations ≤ 2.[38] In line with these results, predictions of 2-styrylchromone derivatives that have potential as oral bioavailability indicate that MT-1 and MT-3 compounds have good potential compared to MT-2 and controls (Fig. 2). The criteria for candidate drugs that have good oral bioavailability, such as lipophility (-0.7 < X LogP3 < 5.0), size (150 D < MW < 500 D), polarity (20 $Å^2$ < TPSA < 130 $Å^2$), insolubility (0 < ESOL < 6), insaturation (0.25 < Csp^3 < 1), and flexibility (0 < number of rotatable bonds < 9).[25] In detail, the oral bioavailability of each compound is G7X: 3 violations (Log S: -6.18, number of rotatable bonds: 10, and XlogP3: 5.33), DM2: 2 violations (MW: 543.52 g/mol and TPSA: 206.07 $Å^2$), MT-1: 0 violation, MT-2: 2 violations (Csp^3: 0.11 and XlogP3: 5.8), and MT-3: 1 violation (Csp^3: 0.11). All findings in this section provide information of 2-styrylchromone derivatives as a potential drug that fulfills several mentioned criteria. It is hoped to list initial considerations in understanding the drug-likeness and bioavailability of 2-styrylchromone derivatives.

The ADMET prediction of the 2-styrylchromone derivatives is well absorbed into the human small intestine (+HIA category) with an HIA value > 90%.[26] Besides, crucial parameters like as the effect of the candidate on the body's metabolic processes indicate that it does not inhibit the activity

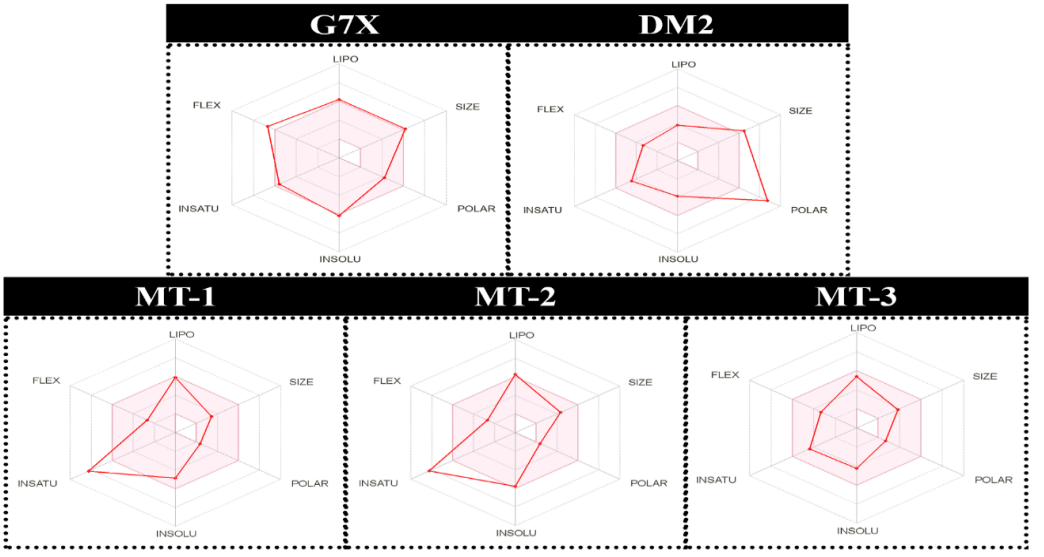

Fig. 2 Oral bioavailability prediction of controls and 2-styrylchromone derivatives.

of cytochrome isoenzymes (CYP), such as CYP2D6 and CYP3A4.[39] Toxicity prediction of MT-1 and MT-3 compounds are not toxic with the criteria of non-AMES toxicity and non-skin sensation. To compare with the control, several obtained information on the 2-styrylchromone derivatives as a drug candidate is listed in Table S2. It should be noted that the prediction results need to be tested in clinical trials. However, the prediction data for ADMET properties can be used as an initial consideration in seeing the ability of 2-styrylchromone derivatives as drug candidates.

3.3 Molecular docking

The molecular docking stage aims to provide the initial coordinates of each inhibitor to the active site of the kinesin Eg5 protein. These stages are in the form of redocking and docking inhibitors with the target protein (kinesin Eg5). The redocking process aims to obtain the coordinates of the protein active site based on the coordinates of the native ligand (Fig. 3A). The redocking criteria show that the G7X superposition value is promising, RMSD: 0.49 Å (Fig. 3B). Then, the docking inhibitors process into the kinesin Eg5 binding site was carried out based on the grid score function. Overall, the grid-score values E_{vdW} + E_{ele} (kcal mol^{-1}) showed a stable interaction for each inhibitor (Fig. 3C).

The docked conformation shows each inhibitor binds well on the Eg5 active site (Fig. 4). According to the Eg5 structure, its active site forms like a pocket that allows small molecules to bind properly. Several amino acid residues in the active site play the Eg5 regulation in the mitosis phase of cancer cell

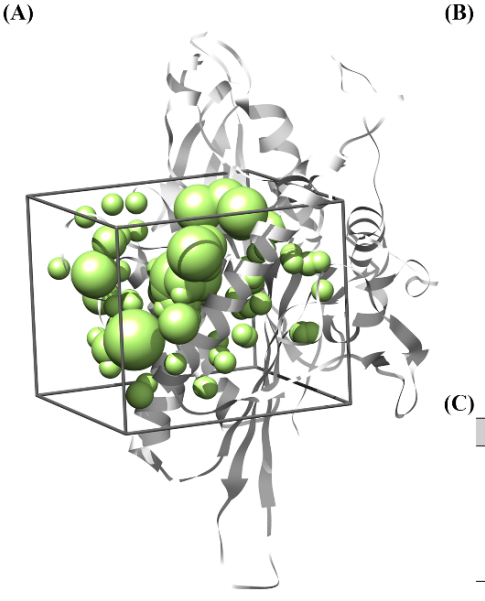

System	Grid-Score	E_{vdW}	E_{ele}
G7X-Eg5	-71.43	-70.70	-0.72
DM2-Eg5	-58.14	-53.33	-4.80
MT-1-Eg5	-39.86	-39.79	-0.06
MT-2-Eg5	-36.83	-37.32	0.49
MT-3-Eg5	-43.41	-41.68	-1.73

Fig. 3 Molecular docking Analysis: (A) Active site preparation: selected sphere and grid-box parameter, (B) Superposition of native ligand (G7X): the native ligand represented by a crystal conformation (black) and rigid conformation (light gray), and (C) The inhibitor-receptor energy (Gas term: E_{vdW} + E_{ele}) was calculated by grid score functional.

growth. Therefore, the presence of an inhibitor on the active site is expected to suppress the Eg5 regulation. Our findings show the binding conformation of 2-styrylchromones has the interaction with several amino acid residues on the active site. Their interaction is visualized in 2D interaction. Overall, the interaction between Eg5 and the inhibitor is provided in several types, such as interaction type, including conventional hydrogen bonds, hydrophobic (π-sigma and π-alky/alkyl/), carbon hydrogen bond, and π-cation/anion. However, these results need to be evaluated by using MD simulations for the conformational dynamics, free energy binding, and decomposition energy of each system.[22] Molecular docking is very useful in determining the initial coordinates of the inhibitor on the active site of the targeted protein by considering time and cost efficiency.[33,40] The obtained coordinates from the molecular docking will be used for further analysis purposes using the MD simulation, which is discussed in the following section.

3.4 Conformational dynamics studies

The trajectories during a simulation time of 100 ns are used to analyze the conformational dynamics of each system in the form of stability, compactness, and flexibility. The analysis of these parameters aims to study the conformational dynamics quality of each system during the simulation. The system that meets the criteria is considered for further analysis, such as water accessibility, binding free energy, energy decomposition, atom contact, and hydrogen bonding.

The root-mean-square displacement (RMSD) of all atoms gives a clear picture of the stability of each system 41. Overall, the fluctuation increased drastically (0-12 ns) and then stabilized slowly until the end of the simulation time (13-100 ns) (Fig. 5). In particular, the last 20 ns trajectories (80-100 ns) showed good RMSD stability of all atoms characterized by low fluctuation. This point needs to be considered in the time range of these trajectories for further analysis purposes. In detail, the RMSD of complex (nm) shows the average value for 100 ns of relatively similar, such as Eg5: 0.28 ± 0.03, G7X-Eg5: 0.27 ± 0.03, DM2-Eg5: 0.31 ± 0.04, MT-1-Eg5: 0.32 ± 0.05, MT-2-Eg5: 0.28 ± 0.03, and MT-3-Eg5: 0.26 ± 0.02. These results describe that the presence of an inhibitor on the active site does not provide significant changes in the kinesin Eg5 structure. This statement is corroborated by looking at the radius of gyration (RoG) data, which has stable fluctuations (Fig. 5) and the average conformation over a simulation time of 100 ns (Fig. 6C). The RoG value gives the idea of the stable folded or not folded.[42] Based on the value of RoG fluctuations, each system was seen to increase to ~2.09 nm. In detail, the mean RoG values of each system, *i.e.*, Eg5: 2.08 ± 0.01, G7X-Eg5: 2.08 ± 0.01, DM2-Eg5: 2.08 ± 0.01, MT-1-Eg5: 2.08 ± 0.01, MT-2-Eg5: 2.08 ± 0.01, and MT-3-Eg5: 2.0 ± 0.00. It indicates that each system has a compact and rigid structure, both Apo protein (without inhibitor) and complex (with inhibitor).

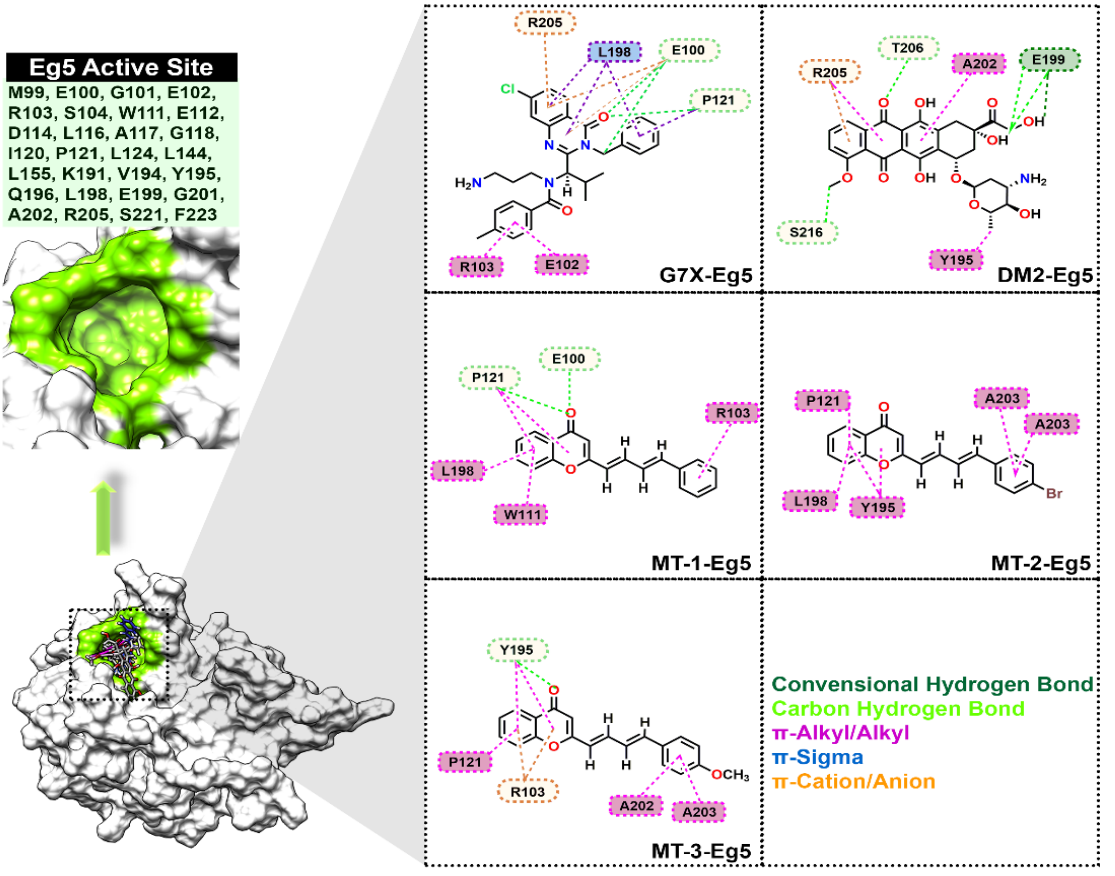

Fig. 4 Molecular docking conformation shows inhibitors bind well on the Eg5 active site (green). The inhibitor-Eg5 interaction is visualized by 2D-interaction types.

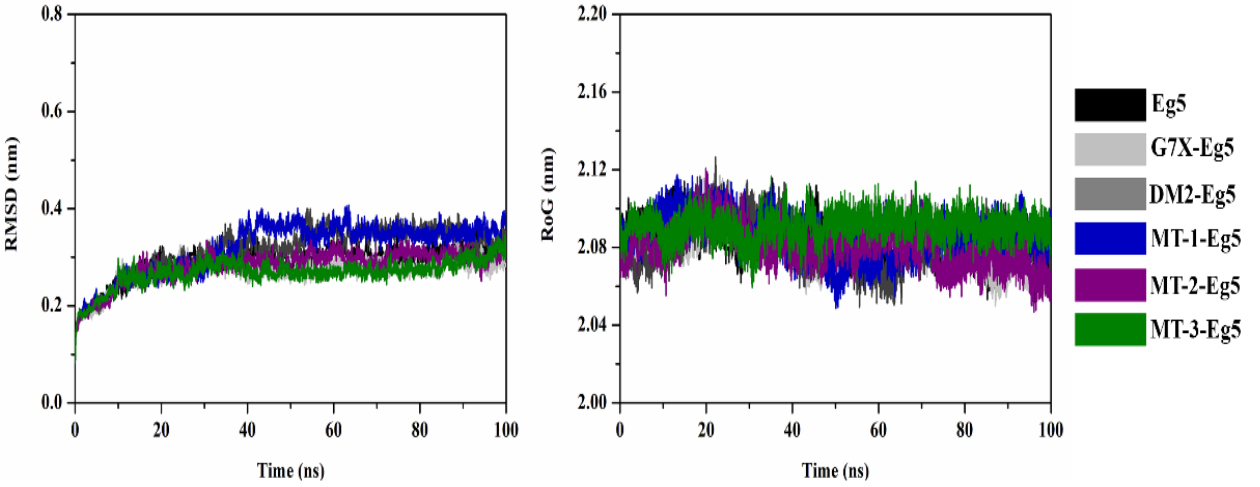

Fig. 5 The root-mean-square displacement of all atoms (left) and radius of gyration (right) for each system plotted along 100 ns of MD simulation.

System flexibility was evaluated through B-factor and the root-mean-square fluctuation (RMSF).[43] Overall, excessive fluctuations occurred in the G7X-Eg5 system (B-factor: 31.92 ± 24.90 nm^2 and RMSF: 10.26 ± 4.06 nm) compared to other systems. The fluctuation occurred in the loops region (number residue: 229-240) (Fig. 6A). Additionally, the fluctuations shown by the B-factor and RMSF give a relatively similar trend in each region. It is supported by the correlation analysis (R2 and R_0^2) between the two parameters, which shows a good correlation value (Fig. 6B). Several previous studies have reported that the relationship between B-factor and RMSF has a strong correlation in looking at the flexibility of a system.[43,44] Therefore, consent to the correlation of these two parameters needs to be presented. It aims to see a more specific fluctuation trend for each amino acid residue. The average conformation of each system during the simulation (100 ns) is presented in the form of a superposition (Fig. 6C).

3.5 Water accessibility

Water accessibility of all surface and active site surface areas are shown in Fig. 7. The water molecule plays a crucial role in mediating the interaction between the inhibitor and the target protein during the simulation time.[45,46] Apo protein has more opportunity to be accessed by water molecules both at all

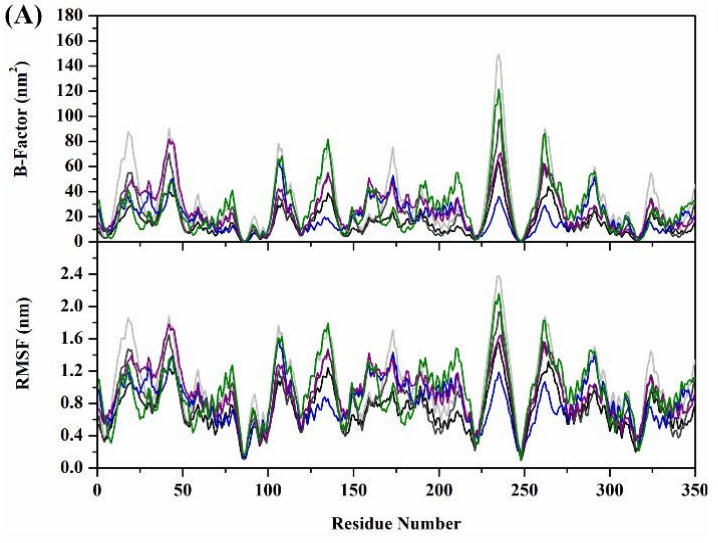

(B)

System	R^2	R_0^2
Eg5	0.94	0.76
G7X-Eg5	0.93	0.75
DM2-Eg5	0.94	0.75
MT-1-Eg5	0.95	0.78
MT-2-Eg5	0.95	0.78
MT-3-Eg5	0.93	0.75

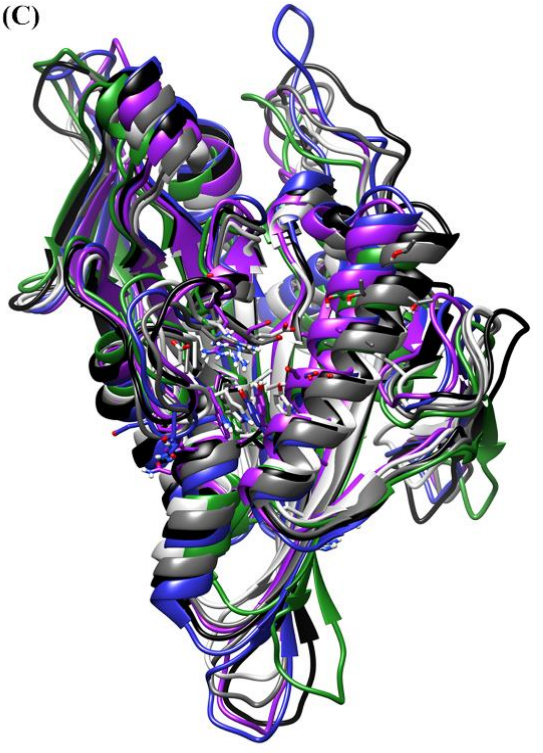

Fig. 6 System flexibility analysis using 100 ns of trajectories: (A) The B-factor and The root-mean-square of fluctuation, (B) The linearity between B-factor and RMSF shown by R2 and R_0^2 (set intercept: 0), and (C) The superposition shown by the average structure of each system.

surfaces (181.64 ± 3.42 nm^2) and active site (12.79 ± 1.02 nm^2). It is natural because the active site pocket does not have an inhibitor that fills that place. Therefore, the opportunity for water molecules to access the active site is higher than other systems with inhibitors. However, this is apart consideration in understanding the ability of water accessibility during the simulation. Meanwhile, systems that contain inhibitors of 2-styrylchromones are the primary consent in this section. Overall, the trend of the solvent-accessible surface area (SASA) for each system is Eg5 > DM2-Eg5 > G7X-Eg5 > MT-3-Eg5 > MT-1-Eg5 > MT-2-Eg5 (Table 1). The results suggest that the water accessibility of the 2-styrylchromones molecules can influence the water molecules in the active site of the kinesin Eg5. In particular, the MT-3-Eg5 system showed a greater chance of water molecule access than the MT-1-Eg5 and MT-2-Eg5 systems. Therefore, modification of the functional group on the benzene ring (B ring) needs to be considered by looking at the hydrophobic property on the kinesin Eg5 active site.

Table 1. The average value of the solvent-accessible surface area using the last 20 ns trajectories.

System	All surface area (nm^2)	Active site surface area (nm^2)
Eg5	181.64 ± 3.42	12.79 ± 1.02
G7X-Eg5	177.57 ± 2.90	10.16 ± 0.67
DM2-Eg5	179.09 ± 3.40	10.77 ± 1.01
MT-1-Eg5	176.66 ± 3.19	8.73 ± 0.93
MT-2-Eg5	174.87 ± 2.94	6.76 ± 0.65
MT-3-Eg5	177.29 ± 3.29	9.65 ± 0.71

3.6 Prediction of binding affinity

Binding free energy (ΔG_{bind}) and decomposition energy ($\Delta G^{residue}_{bind}$) were determined using 100 snapshots extracted from the last 20 ns trajectories using the MM-GBSA approach. The consideration of energy components in gas and solvation terms is listed in Table 2. In this section, we try to describe the interaction between the inhibitor and the kinesin Eg5 in the form of binding affinity as the consideration part in the prediction of efficiency inhibition. It should be noted that G7X and DM2 inhibitors were used as references to see the ability of 2-styryl chromones (MT-1, MT-2, and MT-3) compounds in inhibitory efficiency.

Based on the energy component in the gas phase (ΔG_{gas}), van der Waals energy (E_{vdW}) contributes more profitably than electrostatic energy (E_{ele}). Except, the DM2-Eg5 system shows that the E_{ele} contribution is more profitable than the E_{vdW} contribution. Meanwhile, the energy component of the solvation terms (ΔG_{sol}) shows an unfavorable contribution from the polar terms for Generalized Born models (ΔG^{ele}_{sol}). Assuredly, each energy component affects the total binding free energy (ΔG_{bind}). In our concentration, inhibitors of the 2-styrylchromones showed that MT-2 and MT-3 had a quite promising potential in binding to the active site of the kinesin Eg5. It can be seen from both ΔG_{bind}, which is better (higher negative value) than ΔG_{bind} DM2 as a control. However, both ΔG_{bind} is not better than the native ligand G7X as a known inhibitor of kinesin Eg5. However, these results are sufficient to provide an initial picture of the ability to interact with kinesin Eg5 protein at the molecular level. These results suggest that the modification of functional groups in the benzene ring (B ring) in the form of –Br and $–OCH_3$ has a large effect on ΔG_{bind}. Additionally, inhibitors with good ΔG_{bind} have a higher chance to bind strongly through interaction with amino acid residues on the active site.[47] It is hoped that the inhibitor will be able to stop the activity of the kinesin Eg5, which provides the regulation of mitosis in cancer cells.[12,14,15]

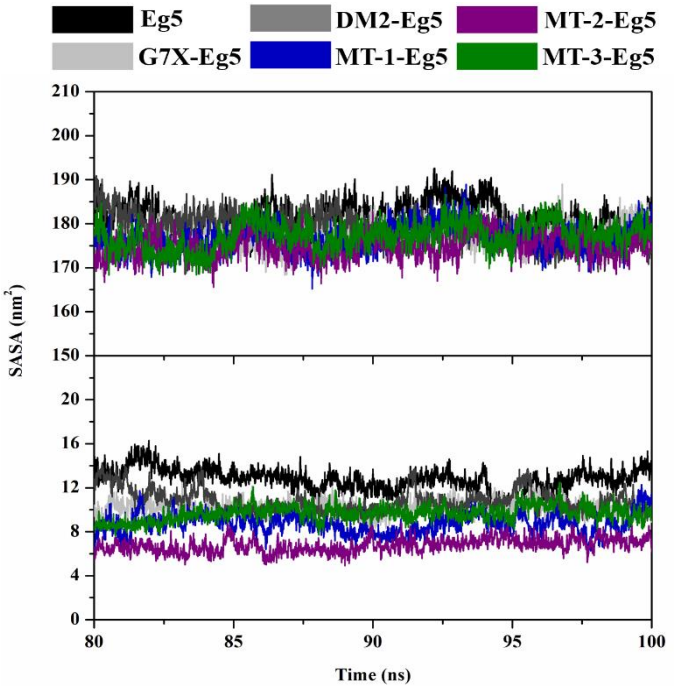

Fig. 7 The solvent-accessible surface area (SASA) using the last 20 ns trajectories: all surface area (top) and active site surface area (bottom). A radius of 5 Å was used to calculate the SASA in the active site of each system.

The inactivation process is carried out by blocking the active site of the kinesin Eg5 protein through interaction with inhibitors. More specifically, the inhibitory mechanism can be studied through the contribution of the energy decomposition ($\Delta G^{residue}_{bind}$) of each amino acid residue to the inhibitor (Fig. 8). The evaluation was only considered by amino acid residues that had a stable contribution to energy decomposition, such as $\Delta G^{residue}_{bind} \leq$ -1.00 kcal mol^{-1}.[48] The results showed that several amino acids were also responsible for the interaction with the inhibitor, *i.e.*, G7X-Eg5 (Eight residues: E100, R103,

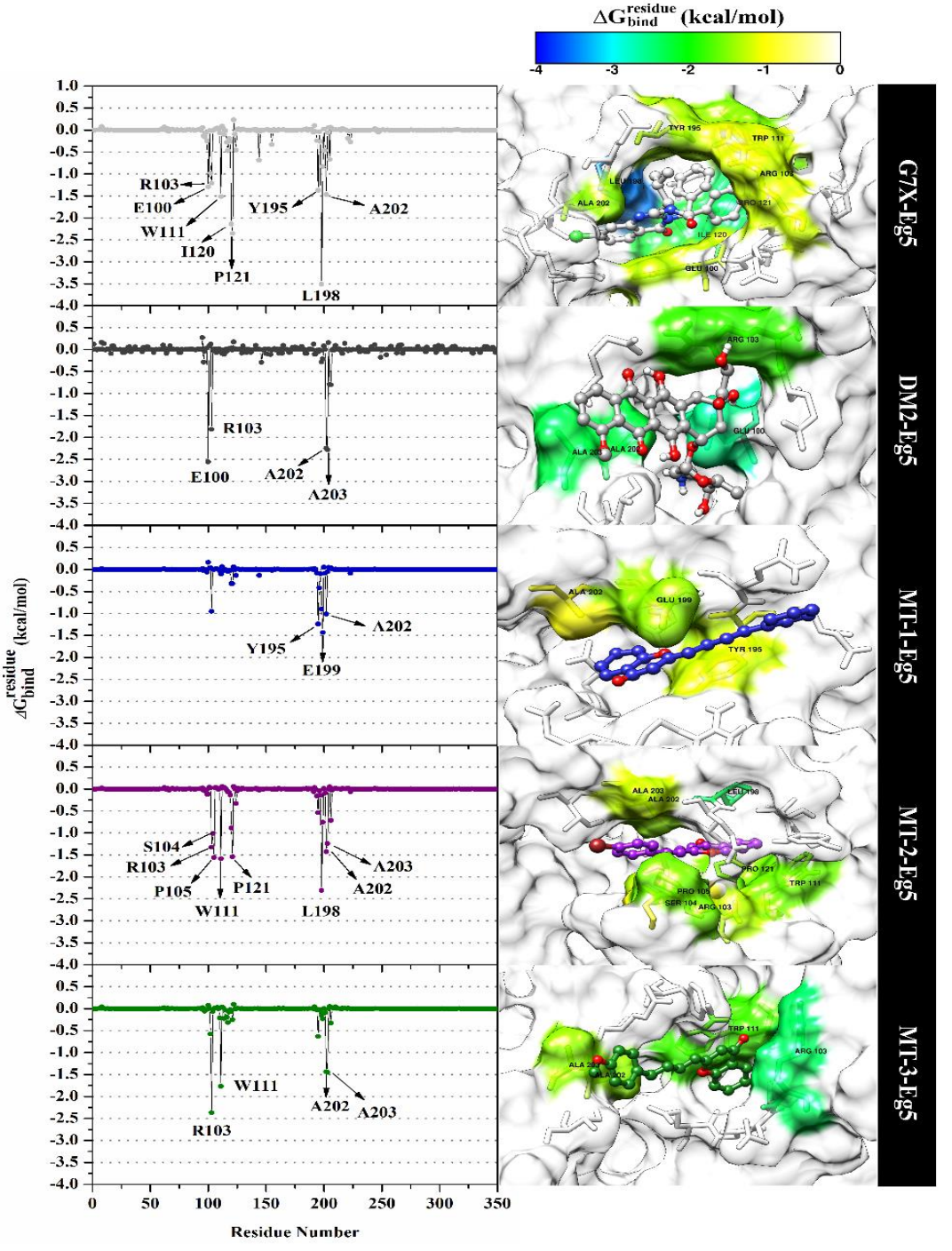

Fig. 8 The energy decomposition performance by the MM-GBSA approach. The results were calculated using the last 20 ns trajectories.

Table 2. Determination of energy component (kcal mol^{-1}) of each complex using the MM-GBSA approach. Data are shown as mean ± standard error of the mean (SEM).

Energy	G7X-Eg5	DM2-Eg5	MT-1-Eg5	MT-2-Eg5	MT-3-Eg5
E_{vdW}	-60.55 ± 0.23	-30.49 ± 0.31	-24.15 ± 0.33	-40.87 ± 0.27	-29.90 ± 0.22
E_{elec}	-6.45 ± 0.33	-155.02 ± 1.52	-2.61 ± 0.33	-15.98 ± 0.28	-6.70 ± 0.21
ΔG_{gas}	-66.00 ± 0.36	-185.51 ± 1.48	-26.76 ± 0.52	-56.86 ± 0.46	-36.61 ± 0.31
ΔG_{solv}^{ele}	25.65 ± 0.32	172.87 ± 1.41	13.65 ± 0.38	28.22 ± 0.30	18.68 ± 0.22
$\Delta G_{solv}^{nonpolar}$	-6.87 ± 0.01	-4.45 ± 0.05	-3.23 ± 0.05	-5.25 ± 0.02	-3.95 ± 0.01
ΔG_{sol}	18.77 ± 0.32	168.42 ± 1.39	10.41 ± 0.36	22.96 ± 0.29	14.72 ± 0.22
ΔG_{bind}	-48.23 ± 0.26	-17.09 ± 0.31	-16.35 ± 0.33	-33.89 ± 0.28	-21.88 ± 0.22

W111, I120, P121, Y195, L198, and A202), DM2-Eg5 (Four residues: E100, R103, A202, and A203), MT-1-Eg5 (Three residues: Y195, E199, and A202), MT-2-Eg5 (Eight residues: R103, S104, P105, W111, P121, L198, A202, and A203), and MT-3 -Eg5 (Four residues: R103, W111, A202, and A203). The obtained results identified that the system with the highest number of amino acid residues with the criteria $\Delta G_{bind}^{residue}$ had a similar correlation with the binding free energy results (Table 2). This assumption can be seen that the G7X-Eg5 and MT-2-Eg5 systems have eight residues with ΔG_{bind} (G7X-Eg5: -48.23 ± 0.26 kcal mol^{-1} and MT3-Eg5: -33.89 ± 0.28 kcal mol^{-1}), which is the most promising compared to other systems. This information becomes an important parameter in understanding the mechanism of interaction between the inhibitor and the Eg5 protein at the molecular level.

3.7 Atomistic interaction on the active site

The previous section discusses the mechanism of inhibition at the molecular level. In this section, we try to describe the atomistic interaction between the inhibitor and the amino acid residue on the active site of the kinesin Eg5. The atomistic analysis was evaluated through atom contact and hydrogen bonding (H-bond) extracted at the last 20 ns trajectories.

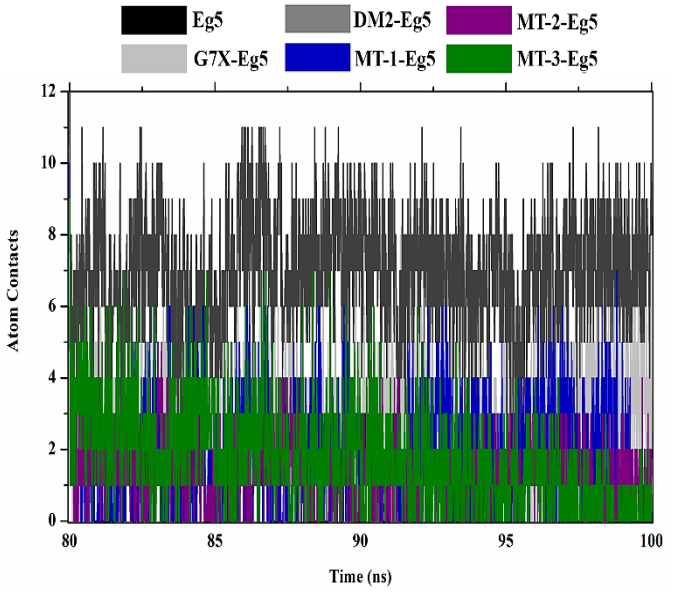

Fig. 9 Atom contacts of each inhibitor on the system.

Atom contact analysis was carried out on amino acid residues at a radius of 3.5 Å with each inhibitor (Fig. 9). In detail, the average value of atom contacts for each system, such as G7X-Eg5 (3 ± 1), DM2-Eg5 (6 ± 2), MT-1-Eg5 (2 ± 1), MT-2-Eg5 (1 ± 0), and MT-3-Eg5 (2 ± 1). More specifically, H-bond analysis plays a crucial role in the inhibitor-Eg5 interaction during the simulation time.[45,46,49] Evaluation of H-bond is carried out on H-bonds that have a fraction of 10%. The analyzed results showed that each inhibitor had a low fraction presentation of < 80% (Table S3). Furthermore, three inhibitors (G7X, MT-1, and MT-2) were not detected by H-bonds with a fraction percentage > 10% during the last 20 ns simulation time. In particular, the MT-3 inhibitor showed one H-bond on the oxygen atom (C=O) with Y195 residue as HBA with a fraction equal to 27.80%. It should be noted that the modification of functional groups on the benzene ring of 2-styrylchromones compounds (B ring) in the form of –Br and –OCH_3 did not contribute more impact on the H-bond interaction. However, these results provide an overview of the consideration of structural modification on the benzene ring (B ring) by adding the number and types of substituents that have the opportunity for H-bond interactions to occur.

4. Conclusions

In the present study, the mechanism of the aldol condensation reaction between 2-methylchromone and various cinnamaldehydes resulted in three compounds, namely 2-((1E,3E)-4-phenylbuta-1,3-dien-1-yl)-4H-chromene-4-on (MT-1), 2-[(1E,3E)-4-(4-bromophenyl)buta-1,3-dien-1-yl)-4H-chromen-4-one (MT-2), and 2-[(1E,3E)-4-(4-methoxyphenyl)blind-1,3-dien-1-yl)-4H-chromen-4-on (MT-3). Meanwhile, the prediction of efficiency inhibition kinesin Eg5 shows that MT-2 and MT-3 have promising potential because they have a stronger ΔG_{bind} than ΔG_{bind} of DM2 as a control. Meanwhile, there are 12 amino acid residues (E100, R103, S104, P105, W111, I120, P121, Y195, L198, E199, A202, and A203), which are responsible for interactions with inhibitors based on criteria $\Delta G_{bind}^{residue} \leq$ -1.00 kcal mol^{-1}. Furthermore, the atomistic level shows that only MT-3 compound has an H-bond (fraction > 10 %), namely C=O…HH-OH(Y195) with weak H-bond category. Besides, pharmacokinetic studies show MT-3 has promising drug-likeness and bioavailability by meeting several regulatory criteria. Moreover, the predicted toxicity results show non-AMES toxicity and non-skin sensitization. The limitation of this research is not performed the in vitro assay to see the potential of of 2-styrylchromone derivatives as kinesin Eg5 inhibitors. Therefore, we highly recommend using the synthesized 2-styrylchromones for in vitro evaluation according to findings provided in this work. It is hoped that the results of the analysis presented in this study can provide information regarding the synthesis of 2-styrylchromone derivatives and their potential as inhibitors of the kinesin Eg5 protein based on computational studies.

Acknowledgements

This research was supported by the Universitas Airlangga "*SKEMA PENELITIAN UNGGULAN AIRLANGGA (PUA) TAHUN 2023*" (Contract number: 293/UN3.15/PT/2023). The authors would like to thank The Bioinformatic Laboratory, UCoE Research Center for Bio-Molecule Engineering Universitas Airlangga, Surabaya, Indonesia is an acknowledgment for providing research and administrative facilities.

Conflict of Interest

There is no conflict of interest.

Supporting Information

Applicable.

References

[1] J. L. Phillips, D. C. Currow, Cancer as a chronic disease, *Collegian*, 2010, **17**, 47-50, doi: 10.1016/j.colegn.2010.04.007.

[2] H. Sung, J. Ferlay, R. L. Siegel, M. Laversanne, I. Soerjomataram, A. Jemal, F. Bray, Global cancer statistics 2020: GLOBOCAN estimates of incidence and mortality worldwide for 36 cancers in 185 countries, *CA: A Cancer Journal for Clinicians*, 2021, **71**, 209-249, doi: 10.3322/caac.21660.

[3] H. Nagai, Y. H. Kim, Cancer prevention from the perspective of global cancer burden patterns, *Journal of Thoracic Disease: Home*, 2017, **9**, 448-451, doi: 10.21037/jtd.2017.02.75.

[4] A. S. Choudhari, P. C. Mandave, M. Deshpande, P. Ranjekar, O. Prakash, Phytochemicals in cancer treatment: from preclinical studies to clinical practice, *Frontiers in Pharmacology*, 2020, **10**, 1-17, doi: 10.3389/fphar.2019.01614.

[5] V. V. Padma, An overview of targeted cancer therapy, *Biomedicine (Taipei)*, 2015, **5**, 1-6, doi: 10.7603/s40681-015-0019-4.

[6] L. Yan, N. Rosen, C. Arteaga, Targeted cancer therapies, *Chinese Journal of Cancer*, 2011, **30**, 1-4, doi: 10.5732/cjc.010.10553.

[7] R. Shahin, S. Aljamal, Kinesin spindle protein inhibitors in cancer: from high throughput screening to novel therapeutic strategies, *Future Science OA*, 2022, **8**, 1-17, doi: 10.2144/fsoa-2021-0116.

[8] Q. Jin, F. Huang, X. Wang, H. Zhu, Y. Xian, J. Li, S. Zhang, Q. Ni, High Eg5 expression predicts poor prognosis in breast cancer, *Oncotarget*, 2017, **8**, 62208-62216, doi: 10.18632/oncotarget.19215.

[9] X. Liu, H. Gong, K. Huang, Oncogenic role of kinesin proteins and targeting kinesin therapy, *Cancer Science*, 2013, **104**, 651-656, doi: 10.1111/cas.12138.

[10] L. Wordeman, How kinesin motor proteins drive mitotic spindle function: Lessons from molecular assays, *Seminars in Cell & Developmental Biology*, 2010, **21**, 260-268, doi: 10.1016/j.semcdb.2010.01.018.

[11] K. Ishikawa, Y. Tamura, S. Maruta, Photocontrol of mitotic kinesin Eg5 facilitated by thiol-reactive photochromic molecules incorporated into the loop L5 functional loop, *The Journal of Biochemistry*, 2014, **155**, 195-206, doi: 10.1093/jb/mvt111.

[12] B. C. Guido, L. M. Ramos, D. O. Nolasco, C. C. Nobrega, B. Y. G. Andrade, A. Pic-Taylor, B. A. D. Neto, J. R. Corrêa, Impact of kinesin Eg5 inhibition by 3,4-dihydropyrimidin-2(1H)-one derivatives on various breast cancer cell features, *BMC Cancer*, 2015, **15**, 1-15, doi: 10.1186/s12885-015-1274-1.

[13] D. Huszar, M.-E. Theoclitou, J. Skolnik, R. Herbst, Kinesin motor proteins as targets for cancer therapy, *Cancer and Metastasis Reviews*, 2009, **28**, 197-208, doi: 10.1007/s10555-009-9185-8.

[14] S. K. Talapatra, A. W. Schüttelkopf, F. Kozielski, The structure of the ternary Eg5–ADP–ispinesib complex, *Acta Crystallographica Section D Biological Crystallography*, 2012, **68**, 1311-1319, doi: 10.1107/s0907444912027965.

[15] A. Gaspar, M. J. Matos, J. Garrido, E. Uriarte, F. Borges, Chromone: a valid scaffold in medicinal chemistry, *Chemical Reviews*, 2014, **114**, 4960-4992, doi: 10.1021/cr400265z.

[16] R. S. Keri, S. Budagumpi, R. K. Pai, R. G. Balakrishna, *European Journal of Medicinal Chemistry*, 2014, **78**, 340-374, doi: 10.1016/j.ejmech.2014.03.047.

[17] S. Demirayak, L. Yurttas, N. Gundogdu-Karaburun, A. C. Karaburun, I. Kayagil, New chroman-4-one/thiochroman-4-one derivatives as potential anticancer agents, *Saudi Pharmaceutical Journal*, 2017, **25**, 1063-1072, doi: 10.1016/j.jsps.2017.04.040.

[18] L. Simon, A. A. Abdul Salam, S. Madan Kumar, T. Shilpa, K. K. Srinivasan, K. Byrappa, Synthesis, anticancer, structural, and computational docking studies of 3-benzylchroman-4-one derivatives, *Bioorganic & Medicinal Chemistry Letters*, 2017, **27**, 5284-5290, doi: 10.1016/j.bmcl.2017.10.026.

[19] R. M. N. Kalla, J. S. Choi, J. W. Yoo, S. J. Byeon, M. S. Heo, I. Kim, Synthesis of 2-amino-3-cyano-4H-chromen-4-ylphosphonates and their anticancer properties, *European Journal of Medicinal Chemistry*, 2014, **76**, 61-66, doi: 10.1016/j.ejmech.2014.02.025.

[20] S. N. Mokale, A. Begum, N. S. Sakle, V. R. Shelke, S. A. Bhavale, Design, synthesis and anticancer screening of 3-(3-(substituted phenyl) acryloyl)-2H-chromen-2ones as selective anti-breast cancer agent, *Biomedicine & Pharmacotherapy*, 2017, **89**, 966-972, doi: 10.1016/j.biopha.2017.02.089.

[21] B. Via Safitri, A. N. Kristanti, H. Suwito, K. Ul Haq, D. Hendriyanto, Synthesis of 2-styrylchromones: In vitro and in silico anticancer activity evaluation, *Journal of Applied Pharmaceutical Science*, 2021, **11**, 121-128, doi: 10.7324/JAPS.2021.110114.

[22] V. Salmaso, S. Moro, Bridging molecular docking to molecular dynamics in exploring ligand-protein recognition process: an overview, *Frontiers in Pharmacology*, 2018, **9**, 1-16, doi: 10.3389/fphar.2018.00923.

[23] T. H. Ogunwa, E. Laudadio, R. Galeazzi, T. Miyanishi, Insights into the Molecular Mechanisms of Eg5 Inhibition by (+)-Morelloflavone, *Pharmaceuticals*, 2019, **12**, 1-19, doi: 10.3390/ph12020058.

[24] I. L. Gonçalves, L. Rockenbach, G. M. Das Neves, G. Göethel, F. Nascimento, L. Porto Kagami, F. Figueiró, G. Oliveira De Azambuja, A. De Fraga Dias, A. Amaro, L. M. De Souza, I. Da Rocha Pitta, D. S. Avila, D. F. Kawano, S. C. Garcia, A. M. O. Battastini, V. L. Eifler-Lima, Effect of N-1 arylation of monastrol on kinesin Eg5 inhibition in glioma cell lines, *MedChemComm*, 2018, **9**, 995-1010, doi: 10.1039/C8MD00095F.

[25] A. Daina, O. Michielin, V. Zoete, SwissADME: a free web tool to evaluate pharmacokinetics, drug-likeness and medicinal chemistry friendliness of small molecules,

Scientific Reports, 2017, **7**, 1–13, doi: 10.1038/srep42717.
[26] D. E. V. Pires, T. L. Blundell, D. B. Ascher, pkCSM: Predicting small-molecule pharmacokinetic and toxicity properties using graph-based signatures, *Journal of Medicinal Chemistry*, 2015, **58**, 4066-4072, doi: 10.1021/acs.jmedchem.5b00104.
[27] C. A. Lipinski, F. Lombardo, B. W. Dominy, P. J. Feeney, Experimental and computational approaches to estimate solubility and permeability in drug discovery and development settings, *Advanced Drug Delivery Reviews*, 2012, **64**, 4-17, doi: 10.1016/j.addr.2012.09.019.
[28] A. K. Ghose, V. N. Viswanadhan, J. J. Wendoloski, A Knowledge-based approach in designing combinatorial or medicinal chemistry libraries for drug discovery. 1. a qualitative and quantitative characterization of known drug databases, *Journal of Combinatorial Chemistry*, 1999, **1**, 55-68, doi: 10.1021/cc9800071.
[29] D. F. Veber, S. R. Johnson, H. Y. Cheng, B. R. Smith, K. W. Ward, K. D. Kopple, Molecular properties that influence the oral bioavailability of drug candidates, *Journal of Medicinal Chemistry*, 2002, **45**, 2615–2623, doi: 10.1021/jm020017n.
[30] W. J. Egan, K. M. Merz, J. J. Baldwin, Prediction of drug absorption using multivariate statistics, *Journal of Medicinal Chemistry*, 2000, **43**, 3867-3877, doi: 10.1021/jm000292e.
[31] I. Muegge, S. L. Heald, D. Brittelli, Simple selection criteria for drug-like chemical matter, *Journal of Medicinal Chemistry*, 2001, **44**, 1841-1846, doi: 10.1021/jm015507e.
[32] O. Tacar, P. Sriamornsak, C. R. Dass, Doxorubicin: an update on anticancer molecular action, toxicity and novel drug delivery systems, *Journal of Pharmacy and Pharmacology*, 2013, **65**, 157-170, doi: 10.1111/j.2042-7158.2012.01567.x.
[33] W. J. Allen, T. E. Balius, S. Mukherjee, S. R. Brozell, D. T. Moustakas, P. T. Lang, D. A. Case, I. D. Kuntz, R. C. Rizzo, DOCK 6: Impact of new features and current docking performance, *Journal of Computational Chemistry*, 2015, **36**, 1132-1156, doi: 10.1002/jcc.23905.
[34] J. Wang, R. M. Wolf, J. W. Caldwell, P. A. Kollman, D. A. Case, Development and testing of a general amber force field, *Journal of Computational Chemistry*, 2004, **25**, 1157-1174, doi: 10.1002/jcc.20035.
[35] D. R. Roe, T. E. Cheatham, PTRAJ and CPPTRAJ: Software for processing and analysis of molecular dynamics trajectory data, *Journal of Chemical Theory and Computation*, 2013, **9**, 3084-3095, doi: 10.1021/ct400341p.
[36] B. R. Miller, T. D. McGee, J. M. Swails, N. Homeyer, H. Gohlke, A. E. Roitberg, MMPBSA.py: An efficient program for end-state free energy calculations, *Journal of Chemical Theory and Computation*, 2012, **8**, 3314-3321, doi: 10.1021/ct300418h.
[37] H. Luo, D. F. Liang, M. Y. Bao, R. Sun, Y. Y. Li, J. Z. Li, X. Wang, K. M. Lu, J. K. Bao, In silico identification of potential inhibitors targeting Streptococcus mutans sortase A, *International Journal of Oral Science*, 2017, **9**, 53-62, doi: 10.1038/ijos.2016.58.
[38] M. Athar, A. N. Sona, B. D. Bekono, F. Ntie-Kang, Fundamental physical and chemical concepts behind "drug-likeness" and "natural product-likeness", *Physical Sciences Reviews*, 2019, **4**, 1–18, doi: 10.1515/psr-2018-0101.
[39] Y. Han, J. Zhang, C. Q. Hu, X. Zhang, B. Ma, P. Zhang, *In silico* ADME and Toxicity Prediction of Ceftazidime and Its Impurities, *Frontiers in Pharmacology*, 2019, **10**, 1–12, doi: 10.3389/fphar.2019.00434.
[40] S. R. Brozell, S. Mukherjee, T. E. Balius, D. R. Roe, D. A. Case, R. C. Rizzo, Evaluation of DOCK 6 as a pose generation and database enrichment tool, *Journal of Computer-Aided Molecular Design*, 2012, **26**, 749-773, doi: 10.1007/s10822-012-9565-y.
[41] I. Aier, P. K. Varadwaj, U. Raj, Structural insights into conformational stability of both wild-type and mutant EZH2 receptor, *Scientific Reports*, 2016, **6**, 1–10, doi: 10.1038/srep34984.
[42] M. Y. Lobanov, N. S. Bogatyreva, O. V. Galzitskaya, Radius of gyration as an indicator of protein structure compactness, *Molecular Biology*, 2008, **42**, 623-628, doi: 10.1134/s0026893308040195.
[43] A. Bornot, C. Etchebest, A. G. de Brevern, Predicting protein flexibility through the prediction of local structures, *Proteins: Structure, Function, and Bioinformatics*, 2011, 79, 839-852, doi: 10.1002/prot.22922.
[44] A. Kuzmanic, B. Zagrovic, Determination of ensemble-average pairwise root mean-square deviation from experimental B-factors, *Biophysical Journal*, 2010, **98**, 861-871, doi: 10.1016/j.bpj.2009.11.011.
[45] V. Ulaganathan, S. K. Talapatra, O. Rath, A. Pannifer, D. D. Hackney, F. Kozielski, Structural insights into a unique inhibitor binding pocket in kinesin spindle protein, *Journal of the American Chemical Society*, 2013, **135**, 2263-2272, doi: 10.1021/ja310377d.
[46] H. Yokoyama, J. I. Sawada, K. Sato, N. Ogo, N. Kamei, Y. Ishikawa, K. Hara, A. Asai, H. Hashimoto, Structural and thermodynamic basis of the enhanced interaction between kinesin spindle protein Eg5 and STLC-type inhibitors, *ACS Omega*, 2018, **3**, 12284-12294, doi: 10.1021/acsomega.8b00778.
[47] E. Wang, H. Sun, J. Wang, Z. Wang, H. Liu, J. Z. H. Zhang, T. Hou, End-point binding free energy calculation with MM/PBSA and MM/GBSA: strategies and applications in drug design, *Chemical Reviews*, 2019, **119**, 9478-9508, doi: 10.1021/acs.chemrev.9b00055.
[48] K. Karnchanapandh, C. Hanpaibool, P. Mahalapbutr, T. Rungrotmongkol, Source of oseltamivir resistance due to single E276D, R292K, and double E276D/R292K mutations in H10N4 influenza neuraminidase, *Journal of Molecular Liquids*, 2021, **326**, 1-7, doi: 10.1016/j.molliq.2021.115294.
[49] S. F. Mousavi, M. H. Fatemi, A combination of molecular docking, receptor-guided QSAR, and molecular dynamics simulation studies of S-trityl-L-cysteine analogues as kinesin Eg5 inhibitors, *Structural Chemistry*, 2019, **30**, 115-126, doi: 10.1007/s11224-018-1178-1.

